ELSEVIER

A theoretical approach to understanding the isotopic heterogeneity of mid-ocean ridge basalt

JOHN F. RUDGE,[1,2,*] DAN MCKENZIE,[1] AND PETER H. HAYNES[2]

[1]Bullard Laboratories, Department of Earth Sciences, University of Cambridge, Madingley Road, Cambridge, CB3 0EZ, UK
[2]Department of Applied Mathematics and Theoretical Physics, Centre for Mathematical Sciences, Wilberforce Road, Cambridge CB3 0WA, UK

Abstract—We have developed an idealized mathematical model to understand the isotopic variability of the mantle and its relation to the observed variations in isotopic ratios $^{143}Nd/^{144}Nd$, $^{87}Sr/^{86}Sr$, $^{176}Hf/^{177}Hf$, $^{208}Pb/^{204}Pb$, $^{206}Pb/^{204}Pb$, and $^{207}Pb/^{204}Pb$ measured on mid-ocean ridge basalt (MORB). We consider a simple box model of mantle processes. A single melt region produces a melt fraction F of melt, and the average time since a given parcel of mantle material last visited this region is given by the time scale τ_{melt}. The melt region fractionates the parent/daughter ratios. Over time this leads to variations in the mantle isotopic ratios as the parent decays to the daughter. Key assumptions are that the half-life of the parent isotope is large compared with τ_{melt}, that the flow is strongly stirring, and that the mantle has reached a statistical steady state. This enables us to neglect the specifics of the underlying flow. Sampling from our model mantle is dealt with by averaging over a large number N of samples to represent the mixing after melting.

The model predicts a probability density for isotopic ratios in MORB which, with exception of the Pb isotopes, are consistent with measurements. Fitting the MORB data to this model gives estimates of the model parameters F, τ_{melt}, and N. Small melt fractions with F around 0.5% are essential for a good fit, whereas τ_{melt} and N are less well constrained. τ_{melt} is estimated at around 1.4 to 2.4 Ga, and N is of the order of hundreds. The model predicts a larger variability for the Pb isotopes than that observed. As has been stated by many previous authors, it appears that fundamental differences exist between the dynamics of Pb isotopes and those of Nd, Sr and Hf isotopes. *Copyright © 2005 Elsevier Ltd*

1. INTRODUCTION

Many measurements of isotopic ratios, such as $^{143}Nd/^{144}Nd$, $^{176}Hf/^{177}Hf$, and $^{87}Sr/^{86}Sr$, have been made on mid-ocean ridge basalt (MORB). These measurements in principle contain significant information on melting and convective processes in the Earth's mantle, but to extract that information requires a suitable quantitative model. In this paper we present a simplified model of what we believe to be the fundamental processes that give rise to the isotopic heterogeneity of MORB. To make the presentation clearer, the paper has been split into two parts. The main text describes the formulation of the model, summarizes the results, and compares them with observations. The appendix presents the mathematical derivations involved.

A good introduction to the geochemical ideas behind this work can be found in the recent reviews by Hofmann (2003) and van Keken et al. (2002). Different approaches have been taken to modelling MORB isotopic measurements. Most work has focused on mixing lines between end member components in the "mantle array" (plots of one isotopic ratio against another). These end members have been classified (White, 1985; Zindler and Hart, 1986), and geochemical models of the Earth have attempted to relate these end members to different parts of the Earth (reservoirs) or different processes occurring in the Earth. Other work has gone further and has attempted to describe the statistical distributions of isotopic ratios (Allègre et al., 1980; Allègre and Lewin, 1995a, b; Kellogg et al., 2002), and this is the main focus of the work we present here. In this

work we will not use reservoir models, and we focus instead on a single statistical mantle source for MORB (Meibom and Anderson, 2003). Important alternative approaches to the work presented here can be found in numerical simulations of mantle convection (Christensen and Hofmann, 1994; Davies, 2002; Ferrachat and Ricard, 2001; Xie and Tackley, 2004), which exploit the same fundamental processes to generate the MORB isotopic heterogeneity.

In this work we have chosen to focus on MORB rather than ocean island basalt (OIB). The main advantage in studying MORB is its statistical uniformity — MORB has similar isotopic characteristics regardless of where in the world it has come from, although there are some small differences between ridges with different spreading rates. Ocean island basalt varies much more from island to island. There are also differences in the melting processes between them. MORB is thought to be produced by passive upwelling with ~10% melt production. OIB is thought to be produced by an active upwelling, with a smaller ~1% melt production. Melting under ocean islands is more complicated to model.

The model we present describes well the isotopes $^{143}Nd/^{144}Nd$, $^{176}Hf/^{177}Hf$, and $^{87}Sr/^{86}Sr$ but not the isotopes of Pb. No attempt is made to model the behaviour of the isotopes of rare gases (such as He, Ne, and Xe).

2. KEY PROCESSES

The isotopic systems we are studying consist of three isotopes, whose molar concentrations we will label as p, d and d'. p is the parent isotope, which decays with decay constant λ to the daughter isotope d. d' is a stable reference isotope of the

* Author to whom correspondence should be addressed (rudge@esc.cam.ac.uk).

same element as d, whose abundance does not change by radioactive decay. It is measurements of isotopic ratios d/d' that are made on MORB.

The heterogeneity of d/d' in the model arises from partial melting processes in the mantle which fractionate the parent element from the daughter element. It is assumed that isotopes of the same element have the same behavior under melting, so the ratio d/d' is unchanged after melting. The fractionation leads to differences in the p/d' ratio of different parts of mantle material. Over time this leads to differences in d/d' as the parent isotope p decays to the daughter isotope d. While melting processes create heterogeneity, they are also responsible for destroying it. When the mantle melts, there is a mixing of different melts, which smooths out the variations in d/d'.

These processes occur on the background of mantle convection and plate tectonics. Mantle convection stirs the mantle and reduces the lengthscale of heterogeneities. The distinction between stirring by the convection, and the mixing of the melts should be emphasised—stirring does not reduce the heterogeneity. The convection also plays a key role in recycling. Melted material comes to the surface to form new crust, which may later become subducted back into the mantle and subsequently undergo further melting events.

Finally, it is important to note that we cannot sample from the mantle directly; we can only do so after it has melted and come to the surface. Therefore we expect the variations we observe in MORB to be less than those in the underlying mantle.

3. THE MODEL

Our model consists of two stages. First, we examine the processes that create and destroy heterogeneity in the mantle to derive the form of the distribution of d/d' in the interior. Second, we examine the processes involved in sampling after melting from this model mantle to predict how this interior distribution relates to a distribution we expect to observe at mid-ocean ridges.

We consider an episodic model with a box representing the mantle. For an interval of time Δt, parcels are advected around the box and the appropriate radioactive decay is followed. At the end of this interval, a melting event occurs. In a melting event we produce a single melt fraction F of melt. We average the concentrations of p, d, and d' in the melting region of the box, and use this to calculate the relevant concentrations in the melt and residue produced. These concentrations depend on the partition coefficients for each isotope, and we assume that isotopes of the same element, such as d and d', have the same behavior under melting. A fraction F of the material in the melting region is then set with the uniform melt value composition, and a fraction $1 - F$ with the uniform residue composition. In this way our melt region both creates and destroys heterogeneity.

In order to simplify the model we make two key assumptions. The first is that the radioactive decay is slow, so that we can linearize the equation of radioactive decay. The second is that the advection is strongly stirring. By this we mean that the stirring is such that the statistics of the melting region at the end of the interval are the same as the statistics over the whole box. This situation gives rise to a statistical steady state (Armstrong,

1968) and a model mantle which is statistically of the same isotopic composition everywhere (although not a uniform composition). For calculational convenience, we also take the limit as $\Delta t \to 0$. An important parameterization of the melting process is then the time scale τ_{melt}, which determines how often on average it has been since an individual parcel last experienced a melting event. The assumption that the radioactive decay is slow is then formally that $\lambda \tau_{\text{melt}} \ll 1$.

It is then possible to derive analytically an expression for the distribution of d/d' in our model mantle (Appendix A).

4. SAMPLING

As mentioned earlier, we cannot sample from the mantle directly but instead sample after melting. To model this we have extended the ideas of "sampling under melting and averaging" (SUMA) of Meibom and Anderson (2003). To model the sampling we mix together a large number N of independent identically distributed samples from our model mantle. N characterises the mixing: If N is large, there is a large amount of mixing between different components and thus a large reduction in the variability observed. N is a simple single parameter characterization of the averaging process, which in practice is determined by a variety of different factors such as the length scale of heterogeneities, the length scale of the mantle region undergoing partial melting, the diffusivity of chemical species in the melt, and the time spent in magma chambers.

In the case of averaging large numbers of independent samples, the central limit theorem is potentially relevant (Allègre and Lewin, 1995b; Meibom and Anderson, 2003). It states that the average of N independent random samples from a distribution with mean μ_0 and standard deviation σ_0 approaches a normal distribution with mean μ_0 and standard deviation $\sigma_0/\sqrt{N}$ as N increases. However, the central limit theorem is not directly applicable to the distribution of the ratio d/d' because it is the individual concentrations d and d' that are averaged and then the ratio d/d' calculated and not the other way round. However, it can be shown that the model d/d' distribution does approach a normal distribution as N increases, but the standard deviation is not simply $\sigma_0/\sqrt{N}$. Appendix B explains the details of calculating the distribution after sampling, and Appendix C considers the large N asymptotics.

5. ANALYTIC RESULTS

For large N there are a number of asymptotic results that can be derived for the properties of the d/d' distribution after sampling. The most important analytic result is for the asymptotic behavior of the standard deviation σ of the distribution:

$$\sigma \approx \lambda \tau_{\text{melt}} \left| G_d - G_p \right| \left(\frac{\bar{p}}{\bar{d}'} \right)_0 \sqrt{\frac{2}{NF(1 - F)}} \qquad (1)$$

Here λ is the decay constant of the parent isotope; $(\bar{p}/\bar{d}')_0$ is the ratio of the mean parent isotope concentration to mean reference isotope concentration over the whole box at the present day; G_p and G_d are functions of the melt fraction F and the relevant partition coefficients, where the lower case subscripts p and d refer to the parent and daughter isotopes under consideration. G is a measure of the incompatibility of a given

Table 1. Given parameters.

parent isotope	p	^{147}Sm	^{87}Rb	^{176}Lu	^{232}Th	^{238}U	^{235}U
daughter isotope	d	^{143}Nd	^{87}Sr	^{176}Hf	^{208}Pb	^{206}Pb	^{207}Pb
reference isotope	d'	^{144}Nd	^{86}Sr	^{177}Hf	^{204}Pb	^{204}Pb	^{204}Pb
decay rate/Ga^{-1}[a]	λ	0.00654	0.0142	0.0193	0.0495	0.155	0.985
parent part. coeff.[b]	D_p	0.03990	0.00039	0.29739	0.00021	0.00054	0.00054
parent part. coeff.[b]	P_p	0.12392	0.00058	0.94719	0.00068	0.00178	0.00178
daughter part. coeff.[b]	D_d	0.02787	0.02983	0.04508	0.02793	0.02793	0.02793
daughter part. coeff.[b]	P_d	0.08653	0.08908	0.14333	0.07175	0.07175	0.07175
mean isotopic par./dau. ratio[c]	$(\bar{p}/\bar{d}')_0$	0.253	0.0188	0.0324	20.0	8.04	0.0583

[a] Decay constants λ of the parent isotopes are accurately known (Faure, 1986). Some λ have been rounded.

[b] Partition coefficients based on the estimates of McKenzie and O'Nions (1991), taking a linear combination of the values for garnet and spinel peridotite (Appendix F).

[c] $(\bar{p}/\bar{d}')_0$ estimated from the depleted mantle model of McKenzie and O'Nions (1991) (Appendix F).

isotope under a particular melt fraction. If $G \approx 0$ then the isotope is compatible (stays in the residue), whereas if $G \approx 1$ then it is incompatible (readily enters the melt). For the Shaw (1970) melting model, G_p is given by

$$G_p = 1 - \left(1 - \frac{P_p}{D_p}F\right)^{1/P_p} \tag{2}$$

where capital P and D are different weighted averages of partition coefficients:

$$D_p = \sum_i x^i K_p^i$$
$$P_p = \sum_i q^i K_p^i \tag{3}$$

K_p^i is the mineral/melt partition coefficient for the parent in mineral i; x^i is the mass fraction of mineral i in the source rock; and q^i is the fractional contribution of mineral i to the melt. G_d is defined similarly.

Some features of the equation for σ can be easily interpreted. Variations in d/d' arise from differences in p/d'. Because we are assuming linearized decay, σ depends linearly on λ and $(\bar{p}/\bar{d}')_0$. Also, because the only other time scale in the problem is τ_{melt} and since σ is nondimensional, then on dimensional grounds we must have a linear dependence on τ_{melt} also. So with larger τ_{melt}, the longer it is between melting events and thus the greater the heterogeneity that can arise.

The role of the melting behaviour on σ is less obvious. The dependence on $|G_d - G_p|$ is indicative of the fact that there has to be a fractionation between parent and daughter to produce the heterogeneity. As such, small melt fractions are essential. For example, large melt fraction MORB melting would have $G \approx 1$ for nearly all elements under consideration and as such can not produce significant heterogeneity. As mentioned earlier, N is indicative of the amount of mixing after melting, so asymptotically we have smaller σ with larger N.

Another analytic result of particular interest is for the skewness parameter γ_1 (Appendix C.1), which measures the asymmetry of the distribution about its mean value:

$$\gamma_1 \approx \frac{3(2G_d - 1)\text{sgn}(G_d - G_p)}{\sqrt{2NF(1 - F)}} \tag{4}$$

Here sgn (x) is the sign function: It equals 1 if x is positive, -1 if x is negative. Hence the sign of the skew is determined by the sign of $(G_d - G_p)(2G_d - 1)$. For example, if $G_p < G_d$ (parent

more compatible than daughter) and $G_d < 1/2$ (a sufficiently small melt fraction, say) then the distribution will be asymptotically negatively skewed. Furthermore, note the dependence on $N F (1 - F)$ in the denominator. Although we may think of N as a large parameter, F is usually small, so the skew and non-normality in the distributions can be quite significant.

It is common in geochemistry to plot one isotopic ratio against another. Consider two isotopic systems (1) and (2) with different parent and daughter elements. Suppose we plot $(d/d')^{(2)}$ against $(d/d')^{(1)}$. For large N, the model predicts that samples lie approximately on a straight line through the mean value and gives a prediction for the gradient $\bar{\beta}$ of this line (Appendix C.3)

$$\bar{\beta} \approx \frac{\lambda^{(2)}\left(G_d^{(2)} - G_p^{(2)}\right)\left(\bar{p}/\bar{d}'\right)_0^{(2)}}{\lambda^{(1)}\left(G_d^{(1)} - G_p^{(1)}\right)\left(\bar{p}/\bar{d}'\right)_0^{(1)}} \tag{5}$$

Thus, if we know the partition coefficients, half lives, and mean parent/daughter isotopic ratios for each system, we can infer a melt fraction from the gradient in plots of $(d/d')^{(2)}$ against $(d/d')^{(1)}$.

This equation simplifies in a particular special case. If the daughter isotopes are of the same element for both systems (for example, both isotopes of lead) then all samples lie precisely on a straight line. If it is also the case that the parent elements are the same (or at least behave similarly under melting such that $G_p^{(1)} \approx G_p^{(2)}$) then the gradient β of this line is independent of the melt model and is simply

$$\beta = \frac{\lambda^{(2)}}{\lambda^{(1)}}\left(\frac{\bar{p}^{(2)}}{\bar{p}^{(1)}}\right)_0 \tag{6}$$

Note that this equation will be valid for ^{208}Pb/^{204}Pb and ^{206}Pb/^{204}Pb but not for ^{207}Pb/^{204}Pb. The short half-life of ^{235}U means the ^{207}Pb/^{204}Pb system does not satisfy the slow decay approximation. As such, this model cannot be used for ^{207}Pb/^{204}Pb. It has been included in the data plots for completeness.

6. COMPARISON WITH OBSERVATIONS

The model has the following input parameters: λ, $(\bar{d}/\bar{d}')_0$, $(\bar{p}/\bar{d}')_0$, P_d, D_p, P_d, D_d, τ_{melt}, F, and N. We are only concerned with studying the variations in d/d', so $(\bar{d}/\bar{d}')_0$ is not important to us. We will choose it appropriately to get a match with the mean of the observations. Other parameters we will base on

estimates by previous authors as shown in Table 1. We assume that the melting takes place somewhere in the garnet-spinel transition region. As such the partition coefficients we have used are a linear combination of the coefficients for garnet and spinel peridotite. With the exception of the Lu-Hf system, there is little difference in the partition coefficients for these two rock types, so the Lu-Hf system was used to constrain this linear combination.

There are just three unknown parameters left in this model: the melting time scale τ_{melt}, the effective melt fraction F producing the heterogeneity, and the parameter N characterizing the mixing before sampling. Note also that these three parameters are independent of the isotopic system under consideration.

6.1. Samarium-Neodymium

The Sm-Nd system is the best constrained of the systems under examination. The Sm/Nd ratio of the bulk Earth is taken to be chondritic, and there is general agreement on the values for the partition coefficients of Sm and Nd (Green, 1994). Therefore, the Sm/Nd ratio in depleted mantle models can be calculated accurately.

6.2. Rubidium-Strontium

The Rb-Sr system is less well constrained. Owing to the volatility of Rb, the bulk Earth Rb/Sr ratio is not precisely known. Furthermore, the observed behavior of Sr under melting is not well described by the partition coefficients that have been measured in the laboratory (Hanson, 1977). Therefore, estimates of Rb/Sr in depleted mantle models vary considerably (for example, a 35% larger estimate than that in Table 1 is given by Salters and Stracke (2004)).

6.3. Lutetium-Hafnium

The Lu-Hf system is similar in many ways to the Sm-Nd system, in that we can get good estimates on the Lu/Hf ratio from chondrites. However, this system is complicated by the large difference between partition coefficients for Lu in the spinel and garnet stability fields. A 37% larger estimate for Lu/Hf is given in Salters and Stracke (2004). Also, fewer measurements of hafnium isotopes have been made.

6.4. Uranium-Thorium-Lead

The U-Th-Pb systems are the most difficult to model. The ratio of U/Pb in the depleted mantle is not well known (discussed later), and the behavior of lead under melting is not well understood (Tatsumoto, 1978; White, 1993).

7. RESULTS

The three parameters F, N, and τ_{melt} were varied in order to fit the model to the measurements of MORB isotopic ratios (sources given in Appendix F).

F is the most straightforward parameter to constrain, if the decay rates, partition coefficients and mean parent/ daughter isotopic ratios are known. Equation 5 shows that the average gradient in plots of one isotopic ratio against another are
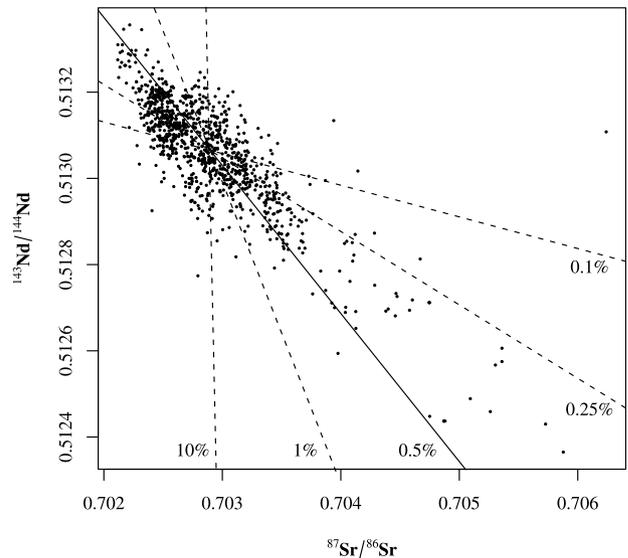

Fig. 1. Plot of ^{143}Nd/^{144}Nd against ^{87}Sr/^{86}Sr. Measured MORB data points are plotted. Straight lines are model predictions using Eqn. 5 with melt fraction F as indicated. A melt fraction of 0.5% provides a good fit.

determined by the melt fraction F and is independent of N or τ_{melt} to leading order. Figure 1 gives an example of such a plot, and shows how F can be varied to provide a good fit. The Sm-Nd and Rb-Sr systems constrain F to be around 0.5%.

N and τ_{melt} are harder to constrain, mainly owing to the dependence on $\tau_{\mathrm{melt}}/\sqrt{N}$ of the standard deviation for large N. Given F, the standard deviations only constrain $\tau_{\mathrm{melt}}/\sqrt{N}$ so a longer time scale could be offset by a large amount of averaging before mixing. Increasing τ_{melt} stretches the density linearly. The variation with N is more complicated, because it also has an effect on the shape of the distributions (Fig. 2). For N large the model distribution approaches a normal distribution, yet there is a definite skew to the distributions that are observed. Therefore, all that can be said with any certainty is that τ_{melt} is around 1.2–2.4 Ga, and N is of the order of hundreds to get a reasonable fit to the data.

Motivated by these constraints, Figures 3 and 4 compare the measurements with model data using $F = 0.5\%$, $\tau_{\mathrm{melt}} = 1.7$ Ga and $N = 500$. Fig. 3 shows a plot of kernel-smoothed probability density estimates for model and measured data. Kernel-smoothed density estimates (Appendix D) are a generalization and improvement on histograms. They have the advantage of being smooth, and have no dependence on the endpoints of bins as histograms do. They do have a dependence on the bandwidth of the kernel, which determines how smoothed out distribution features become. However, there are algorithms for choosing the most appropriate bandwidth, and these have been used. Fig. 4 shows a more traditional set of scatterplots for pairs of the isotopic systems. These plot an artificial sample from the model, as well as the measured data. Table 2 lists the values of a few important calculated parameters.

In Table 2, $G_d < 1/2$ for all isotopic systems. Therefore, Eqn. 4 implies that the sign of the skew is determined by the sign of $G_d - G_p$, i.e., by the relative compatibility of parent and daughter. Where the parent is more compatible than the daugh-
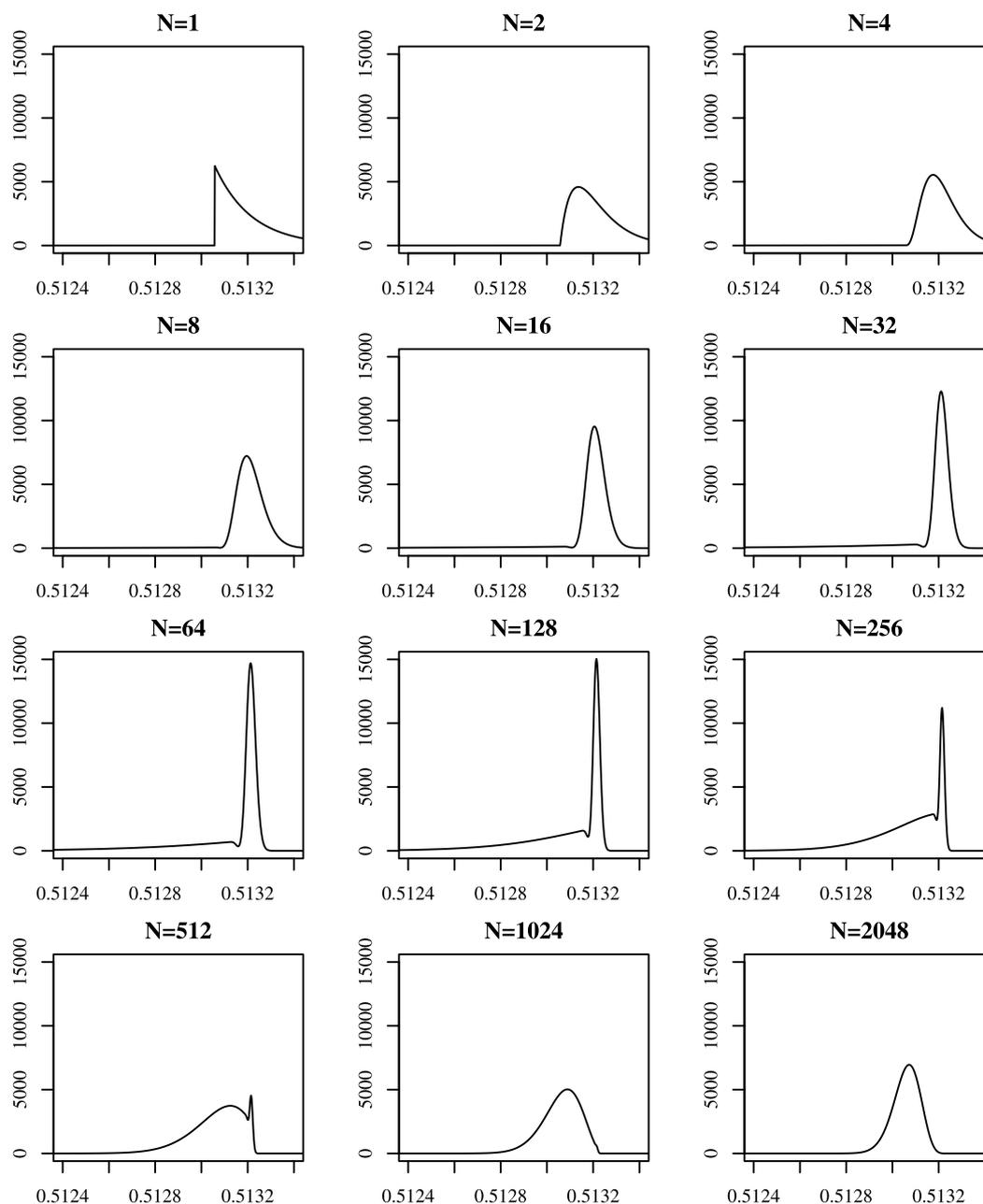
Fig. 2. Plot of model probability densities for ^{143}Nd/^{144}Nd with $F = 0.5\%$, $\tau_{\mathrm{melt}} = 1.7$ Ga, and N varied as shown. Surprisingly, for N between 2 and 30 the standard deviation actually increases as N is increased. For large N the distribution becomes more symmetric and gaussian in appearance, and the standard deviation decreases as $1/\sqrt{N}$ (Eqn. 1). $N = 500$ gives a similar distribution shape to that observed (Fig. 3). Note that $(\bar{d}/\bar{d}')_0$ has been chosen to match the observed mean with $N = 500$.

ter ($G_d - G_p > 0$, e.g. Sm-Nd, Lu-Hf) we expect a negatively skewed distribution, and where the parent is less compatible ($G_d - G_p < 0$, e.g. Rb-Sr, U-Th-Pb) a positively skewed distribution. This is what is observed. Note also that $N F (1 - F) = 2.5$, so that the skews and the non-normality in these distributions are appreciable. Furthermore, note that the sign of the correlations in the plots of one isotope against another is given by $(G_d - G_p)^{(2)}/(G_d - G_p)^{(1)}$, and thus the observed

correlations are also governed by the relative compatibilities of parent and daughter elements.

The special case that yields Eqn. 6 applies to the plot of ^{206}Pb/^{204}Pb against ^{208}Pb/^{204}Pb. In this case the model predicts a single straight line whose gradient β depends only on the decay constants of ^{238}U and ^{232}Th and on κ, the average isotopic ratio ^{232}Th/^{238}U in the model mantle ($\beta = (\lambda_{232}/ \lambda_{238})\kappa$). Because the decay constants are known, the slope of
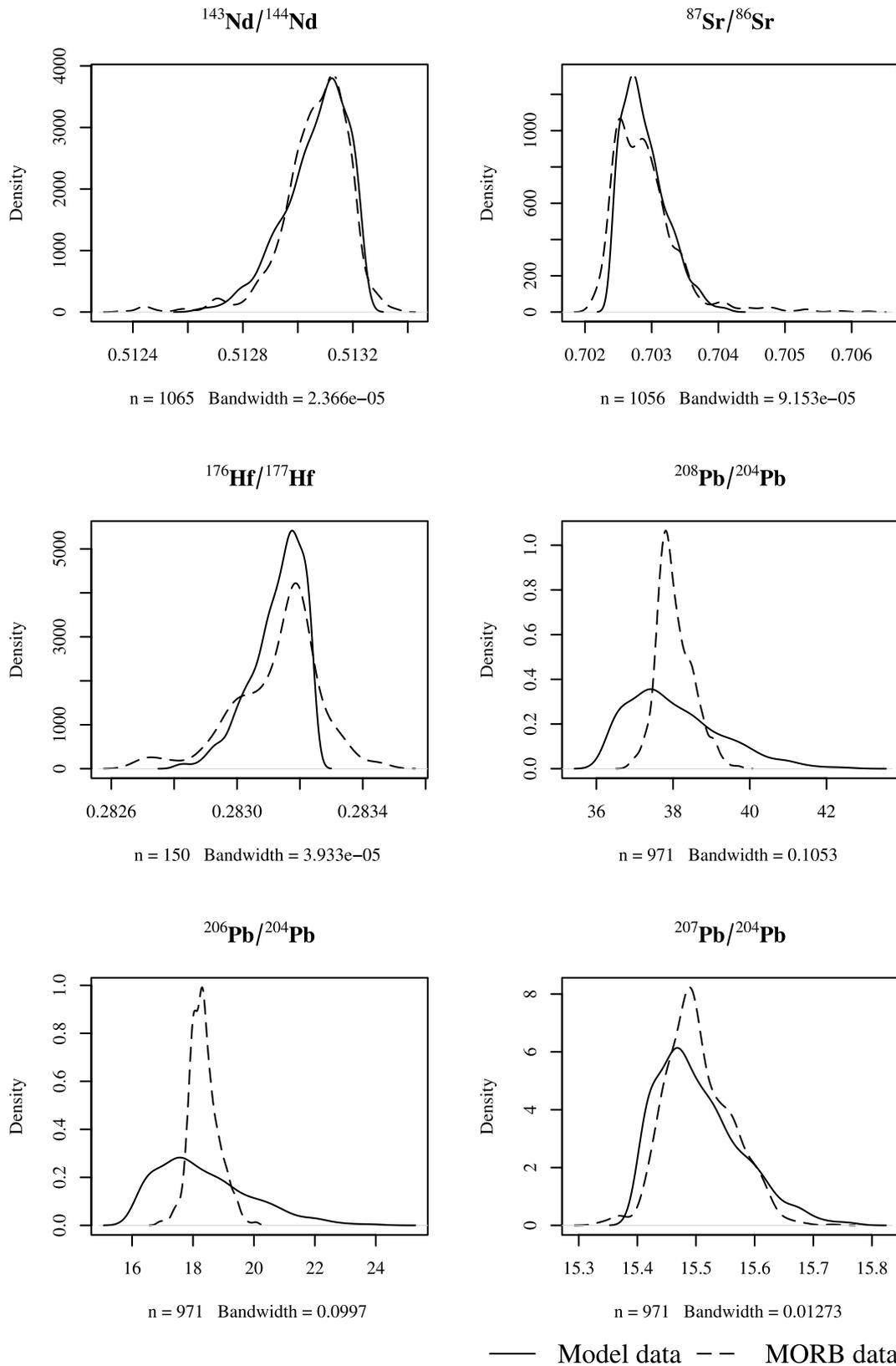
Fig. 3. Plots of kernel-smoothed probability density estimates for model and observed MORB data. *n* gives the number of measured MORB isotopic ratios. The model curves were calculated from a sample of size 1000 generated by numerical simulation. The bandwidth quoted is the standard deviation of the gaussian kernel smoother applied.
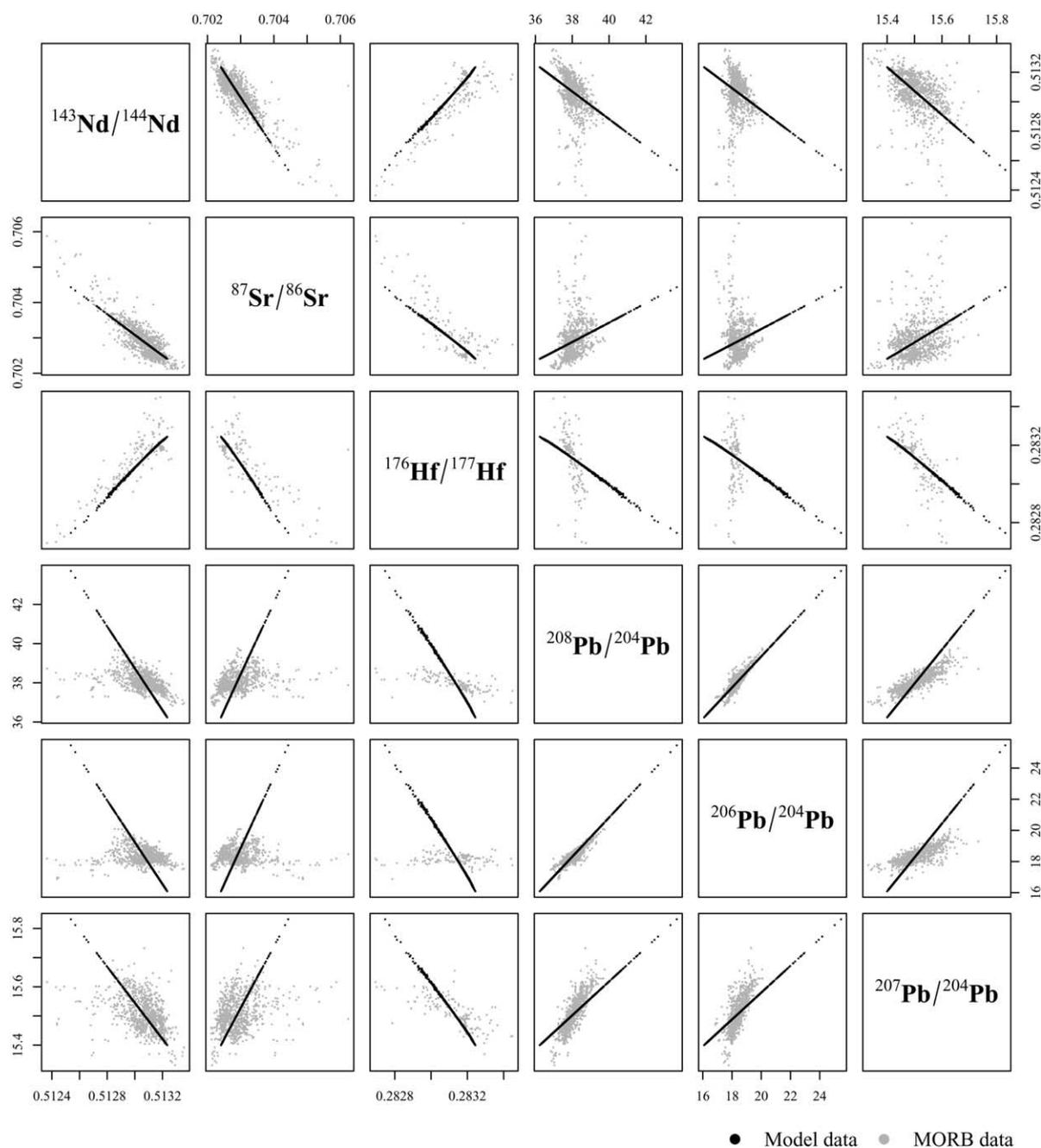
Fig. 4. Scatter plots of model and observed MORB data.

the plot of $^{206}Pb/^{204}Pb$ against $^{208}Pb/^{204}Pb$ can be used to estimate κ. The value of κ used was 2.5, and this provides a reasonable fit to the observed slope.

There is reasonably good agreement between the model and the measurements of Nd, Sr, and Hf isotopic ratios. The MORB data shows more scatter than the model, but the general trends are the same. Such scatter could possibly be accounted for by the variability in melt fractions in the real mantle. The Pb isotopes, however, do not fit this simple model. The standard deviation of Pb calculated from the model is larger than that observed. An ad hoc solution to this problem is to reduce the average ratio $^{238}U/^{204}Pb$, μ, while keeping κ unchanged. A

value for mean depleted mantle μ of around 2.7 (as opposed to the value of 8.0 used) gives a good match with these parameters. There is still much debate on the value of μ in the depleted mantle, with some authors arguing it should be less than 4.7 (White, 1993) or as high as 14.4 (Salters and Stracke, 2004).

The isotopes of Nd, Sr, and Hf correlate well with each other. The isotopes of Pb also correlate well with each other. But there is little correlation between the isotopes of Nd, Sr, and Hf and the isotopes of Pb. It is important to note that the model Pb isotopes are more variable than the measured. This implies it is not necessary to include additional mechanisms for producing heterogeneity, such as subducted sediments, to explain the

Table 2. Calculated parameters given $F = 0.5\%$, $T_{\text{melt}} = 1.7$ Ga, and $N = 500$.

		^{147}Sm	^{87}Rb	^{176}Lu	^{232}Th	^{238}U	^{235}U
parent isotope	p	^{147}Sm	^{87}Rb	^{176}Lu	^{232}Th	^{238}U	^{235}U
daughter isotope	d	^{143}Nd	^{87}Sr	^{176}Hf	^{208}Pb	^{206}Pb	^{207}Pb
reference isotope	d'	^{144}Nd	^{86}Sr	^{177}Hf	^{204}Pb	^{204}Pb	^{204}Pb
parent incompatibility	G_p	0.119	1.000	0.017	1.000	1.000	1.000
daughter incompatibility	G_d	0.165	0.155	0.106	0.165	0.165	0.165
relative compatibility	$G_d - G_p$	0.047	−0.845	0.089	−0.835	−0.835	−0.835
model asymptotic s.d.[a]	σ_{asym}	1.18×10^{-4}	3.43×10^{-4}	8.49×10^{-5}	1.260	1.587	0.073
MORB data s.d.[b]	σ_{MORB}	1.26×10^{-4}	4.93×10^{-4}	1.36×10^{-4}	0.464	0.469	0.056

[a] σ_{asym} is the asymptotic standard deviation of the model calculated using Eqn. 1.
[b] σ_{MORB} is the standard deviation of the isotopic measurements on MORB.

observed variations. Note also that Sm, Nd, Lu, and Hf are elements which are little depleted in the mantle by the formation of continental crust. Sr is also only little depleted, but its parent, Rb, is very depleted. Th, U, and Pb are all much depleted in the mantle by the formation of continental crust. As has been stated by many previous authors, the dynamics of the Pb systems seem notably different to those of Nd, Sr and Hf.

8. PREVIOUS WORK

There has been some recent work done on this problem by other authors. Most recently, Meibom and Anderson (2003) introduced the ideas of the statistical upper mantle assemblage and of sampling under melting and averaging (which they refer to as SUMA). Their ideas form a key part of the model we present here. The only slight criticism we have of their work is in their assessment of the standard deviation within the framework of the central limit theorem (see Appendix E for a fuller discussion). Their paper describes the ideas behind SUMA, argues strongly for statistical ways of thinking about these distributions, and discusses in more detail possible interpretations of the mixing parameter N (referred to as M in that paper).

Another detailed examination of this problem was recently given by Kellogg et al. (2002). Many of the main ideas in their modeling approach are shared with our own. They too have partial melting as the primary cause of heterogeneity and have a sampling process that averages different components in their model mantle to reduce heterogeneity. The main difference in the two approaches lies in their complexity. The Kellogg et al. (2002) model analyzes the behavior of multiple reservoirs with fluxes between them, whereas our model looks at essentially just one statistical depleted mantle reservoir. Their model has to track subreservoirs within these reservoirs to study the heterogeneity and further sub-subreservoirs to handle the sampling. As such, in order to implement their model it is necessary to solve numerous differential equations numerically. Furthermore, their approach leads to a proliferation of unknown free parameters, even more so in extensions of their model to fit Pb data (Kellogg, 2004). Their findings for the Sm-Nd and Rb-Sr systems are broadly similar to our own, and importantly they also found that small melt fractions (also around 0.5%) were essential to getting a good fit to the data. The advantage of our model is that it is able to reproduce such features using a simpler and analytically tractable framework with just a few free parameters.

Modeling mixing by averaging N components was used for trace element observations by Slater et al. (2001). The variability in trace elements in the Slater et al. (2001) model arises

from mixing between different fractional melts from a uniform MORB source. They found the standard deviation of their model fractional melts to be a factor of 4 greater than that observed in melt inclusions, which in turn was a factor of 4 greater than that observed in the host lavas. Thus their $N \approx 16^2 \approx 250$, which is of similar magnitude to our model. However, our model differs in using a heterogeneous MORB source, which is necessary when studying isotopic variability rather than elemental.

A number of the important ideas in this paper can be found in the earlier work of Allègre and Lewin (1995a, b). The first of these papers (Allègre and Lewin, 1995a) stresses the importance of looking at the distributions of geochemical measurements and examines in general terms how various distributions can arise from the fundamental processes of mixing and fractionation. In the context of this paper the model mantle we consider is "a well stirred homogeneous mixture of components from heterogeneous sources." We have heterogeneity in our source components because we have melt and residue components of varying ages. These are strongly stirred in our model mantle and then mixed in the melting before sampling. Importantly, Allègre and Lewin (1995a) stress the role of the central limit theorem and the approach to a normal distribution in such a case.

The subsequent paper (Allègre and Lewin, 1995b) models the standard deviation of isotopic ratios in terms of these fundamental processes. Similar approximations are made as in the work presented here, including looking at a steady state, and linearizing the radioactive decay. However, Allègre and Lewin (1995b) do not distinguish clearly between the distinct processes of stirring and mixing, so direct comparison between the stirring time scale of their paper and the melting time scale of our paper cannot be made. Furthermore, as has been demonstrated in our paper, the behavior of the standard deviation of ratios can be quite nonintuitive and cannot be modeled by a simple linear evolution equation as is done in their paper.

9. CONCLUSIONS

The minimal model we present here goes some way to explaining the isotopic heterogeneity we see in MORB. In this model the heterogeneity in the model mantle is produced by a small melt fraction (0.5%) partial melting process, where on average a parcel of mantle material undergoes such melting around every 2 Ga. In particular, the heterogeneity we observe in MORB does not originate in the large melt fraction melting that produces MORB. One possible place for a small melt

fraction partial melting process to occur to generate this heterogeneity would be underneath ocean island hot spots.

The simplified model does not fit well with the lead isotopes, but this is unsurprising because lead isotopes are generally inconsistent with simple evolutionary models of the depleted mantle. Any resolutions of the various "lead paradoxes" (Galer and O'Nions, 1985; Murphy et al., 2002) should also be able to explain the variability found in the isotopic measurements. The main message here is one of consistency. With the exception of lead, the heterogeneity we see is consistent with a simple model of mantle processes.

The model we have presented is minimal, and neglects many processes that have been proposed to account for the isotopic variability of the mantle. But we hope it contains the most essential physics. There are many possible extensions. Of particular interest would be an extension to the isotopic measurements made on ocean island basalt (OIB). Meibom and Anderson (2003) have argued it may be possible to explain these observations using the same sample source as for MORB but with modifications to the sampling process. For example, there could be a different amount of mixing (a different N), or there could be preferential melting of different components. Preferential melting would require some modifications to the sampling procedures we have described. Real mantle melting takes place at a wide range of melt fractions, so another useful extension would be to consider multiple melt regions with different melt fractions and the effect this would have on the distributions. Another simplifying assumption in this model was in taking a strong stirring statistical steady state, but it is not clear how valid an assumption this is to make. Fluid dynamics simulations may be able to play an important role in examining the validity of this assumption. Further investigation is needed.

Associate editor: Stephen Galer

REFERENCES

Allègre C. J. and Lewin E. (1995a) Scaling laws and geochemical distributions. *Earth Planet. Sci. Lett.* **132,** 1–13.

Allègre C. J. and Lewin E. (1995b) Isotopic systems and stirring times of the earth's mantle. *Earth Planet. Sci. Lett.* **136,** 629–646.

Allègre C. J., Brévart O., Dupré B., and Minister J.-F. (1980) Isotopic and chemical effects produced in a continuously differentiating convecting Earth mantle. *Phil. Trans. R. Soc. Lond.* **297,** 447–477.

Armstrong R. L. (1968) A model for the evolution of strontium and lead isotopes in a dynamic earth. *Rev. Geophys.* **6,** 175–199.

Bach W., Hegner E., Erzinger J., and Satir M. (1994) Chemical and isotopic variations along the superfast spreading East Pacific Rise from 6°S to 30°S. *Contrib. Mineral. Petr.* **116,** 365–380.

Blinnikov S. and Moessner R. (1998) Expansions for nearly gaussian distributions. *Astron. Astrophys. Suppl. Ser.* **130,** 193–205.

Chauvel C. and Blichert-Toft J. (2001) A hafnium isotope and trace element perspective on melting of the depleted mantle. *Earth Planet. Sci. Lett.* **190,** 137–151.

Christensen U. R. and Hofmann A. W. (1994) Segregation of subducted oceanic crust in the convecting mantle. *J. Geophys. Res.* **99,** 19867–19884.

Davies G. F. (2002) Stirring geochemistry in mantle convection models with stiff plates and slabs. *Geochim. Cosmochim. Acta* **66,** 3125–3142.

Dosso L., Bougault H., Beuzart P., Calvez J. Y., and Joron J. L. (1988) The geochemical structure of the Southeast Indian Ridge. *Earth Planet. Sci. Lett.* **88,** 47–59.

Dosso L., Hanan B. B., Bougault H., Schilling J. G., and Joron J. L. (1991) Sr-Nd-Pb geochemical morphology between 10°N and 17°N on the Mid-Atlantic Ridge—A new MORB isotope signature. *Earth Planet. Sci. Lett.* **106,** 29–43.

Dosso L., Bougault H., and Joron J. L. (1993) Geochemical morphology of the North Mid-Atlantic Ridge, 10°–24°N—Trace element–isotope complementarity. *Earth Planet. Sci. Lett.* **120,** 443–462.

Dosso L., Bougault H., Langmuir C., Bollinger C., Bonnier O., and Etoubleau J. (1999) The age and distribution of mantle heterogeneity along the Mid-Atlantic Ridge (31–41°N). *Earth Planet. Sci. Lett.* **170,** 269–286.

Douglass J., Schilling J. G., and Fontignie D. (1999) Plume-ridge interactions of the Discovery and Shona mantle plumes with the Southern Mid-Atlantic Ridge (40°–55°S). *J. Geophys. Res.-Solid.* **104,** 2941–2962.

Faure G. (1986) *Principles of Isotope Geology*, 2nd edition Wiley.

Ferrachat S. and Ricard Y. (2001) Mixing properties in the Earth's mantle: Effects of the viscosity stratification and of oceanic crust segregation. *Geochem. Geophys. Geosyst.* **2,** doi:10.1029/2000GC000092.

Fontignie D. and Schilling J. G. (1996) Mantle heterogeneities beneath the South Atlantic: A Nd-Sr-Pb isotope study along the Mid-Atlantic Ridge (3°S–46°S). *Earth Planet. Sci. Lett.* **142,** 209–221.

Frey F., Walker N., Stakes D., Hart S., and Nielsen R. (1993) Geochemical characteristics of basaltic glasses from the Amar and FAMOUS Axial Valleys, MidAtlantic Ridge (36°–37°N)—Petrogenetic implications. *Earth Planet. Sci. Lett.* **115,** 117–136.

Galer S. J. G. and O'Nions R. K. (1985) Residence time of thorium, uranium and lead in the mantle with implications for mantle convection. *Nature* **316,** 778–782.

Green T. H. (1994) Experimental studies of trace-element partitioning applicable to igneous petrogenesis: Sedona 16 years later. *Chem. Geol.* **117,** 1–36.

Hamelin B. and Allègre C. J. (1985) Large-scale regional units in the depleted upper mantle revealed by an isotope study of the southwest Indian Ridge. *Nature* **315,** 196–199.

Hamelin B., Dupre B., and Allègre C. J. (1986) Pb-Sr-Nd isotopic data of IndianOcean Ridges—New evidence of large-scale mapping of mantle heterogeneities. *Earth Planet. Sci. Lett.* **76,** 288–298.

Hanan B. B., Kingsley R. H., and Schilling J. G. (1986) Pb isotope evidence in the South-Atlantic for migrating ridge hotspot interactions. *Nature* **322,** 137–144.

Hanson G. N. (1977) Geochemical variation of sub-oceanic mantle. *J. Geol. Soc. Lond.* **134,** 235–53.

Hegner E. and Tatsumoto M. (1987) Pb, Sr, and Nd isotopes in basalts and sulphides from the Juan-de-Fuca Ridge. *J. Geophys. Res.-Solid.* **92,** 11380–11386.

Hofmann A. W. (2003) Sampling mantle heterogeneity through oceanic basalts: Isotopes and trace elements. In *Treatise on Geochemistry* (eds. H. Holland and K. K. Turekian), Vol. 2, pp. 61–101. Elsevier-Pergamon, Oxford.

Ito E., White W. M., and Gopel C. (1987) The O, Sr, Nd and Pb isotope geochemistry of MORB. *Chem. Geol.* **62,** 157–176.

Kellogg J. B. (2004) *Towards an Understanding of Chemical and Isotopic Heterogeneity in the Earth's Mantle.* Ph.D. thesis, Harvard University.

Kellogg J. B., Jacobsen S. B., and O'Connell R. J. (2002) Modelling the distribution of isotopic ratios in geochemical reservoirs. *Earth Planet. Sci. Lett.* **204,** 183–202.

Kempton P. D., Fitton J. G., Saunders A. D., Nowell G. M., Taylor R. N., Hardarson B. S., and Pearson G. (2000) The Iceland plume in space and time: A Sr-NdPb-Hf study of the North Atlantic rifted margin. *Earth Planet. Sci. Lett.* **177,** 255–271.

Klein E. M., Langmuir C. H., Zindler A., Staudigel H., and Hamelin B. (1988) Isotope evidence of a mantle convection boundary at the Australian-Antarctic discordance. *Nature* **333,** 623–629.

Klein E. M., Langmuir C. H., and Staudigel H. (1991) Geochemistry of basalts from the Southeast Indian Ridge, 115°E–138°E. *J. Geophys. Res.-Solid.* **96,** 2089–2107.

Lide D. R. (2003) *CRC Handbook of Chemistry and Physics,* 84th CRC Press. edition.

MacDougall J. D. and Lugmair G. W. (1986) Sr and Nd isotopes in basalts from the East Pacific Rise—Significance for mantle heterogeneity. *Earth Planet. Sci. Lett.* **77,** 273–284.

Mahoney J. J., Natland J. H., White W. M., Poreda R., Bloomer S. H., Fisher R. L., and Baxter A. N. (1989) Isotopic and geochemical provinces of the Western Indian-Ocean spreading centers. *J. Geophys. Res.-Solid.* **94,** 4033–4052.

Mahoney J. J., Sinton J. M., Kurz M. D., MacDougall J. D., Spencer K. J., and Lugmair G. W. (1994) Isotope and trace-element characteristics of a super-fast spreading ridge—East Pacific Rise, 13–23°S. *Earth Planet. Sci. Lett.* **121,** 173–193.

Mahoney J. J., Graham D. W., Christie D. M., Johnson K. T. M., Hall L. S., and Vonderhaar D. L. (2002) Between a hotspot and a cold spot: Isotopic variation in the Southeast Indian Ridge asthenosphere, 86°E–118°E. *J. Petrol.* **43,** 1155–1176.

McKenzie D. and O'Nions R. K. (1991) Partial melt distributions from inversion of rare earth element concentrations. *J. Petrol.* **32,** 1021–1091.

Meibom A. and Anderson D. L. (2003) The statistical upper mantle assemblage. *Earth Planet. Sci. Lett.* **217,** 123–139.

Mertz D. F. and Haase K. M. (1997) The radiogenic isotope composition of the high-latitude North Atlantic mantle. *Geology* **25,** 411–414.

Mertz D. F., Devey C. W., Todt W., Stoffers P., and Hofmann A. W. (1991) Sr-NdPb isotope evidence against plume asthenosphere mixing north of Iceland. *Earth Planet. Sci. Lett.* **107,** 243–255.

Michard A., Montigny R., and Schlich R. (1986) Geochemistry of the mantle beneath the Rodriguez triple junction and the Southeast Indian Ridge. *Earth Planet. Sci. Lett.* **78,** 104–114.

Murphy D. T., Kamber B. S., and Collerson K. D. (2002) A refined solution to the first terrestrial Pb-isotope paradox. *J. Petrol.* **44,** 39–53.

Newsom H. E., White W. M., Jochum K. P., and Hofmann A. W. (1986) Siderophile and chalcophile element abundances in oceanic basalts, Pb-isotope evolution and growth of the Earth's core. *Earth Planet. Sci. Lett.* **80,** 299–313.

Price R. C., Kennedy A. K., Riggssneeringer M., and Frey F. A. (1986) Geochemistry of basalts from the Indian-Ocean triple junction—Implications for the generation and evolution of Indian-Ocean ridge basalts. *Earth Planet. Sci. Lett.* **78,** 379–396.

Pyle D. G., Christie D. M., and Mahoney J. J. (1992) Resolving an isotopic bound-ary within the Autralian-Antarctic Discordance. *Earth Planet. Sci. Lett.* **112,** 161–178.

R Development Core Team (2004) *R: A Language and Environment for Statistical Computing.* R Foundation for Statistical Computing, Vienna, Austria. Available at: http://www.R-project.org.

Rehkämper M. and Hofmann A. W. (1997) Recycled ocean crust and sediment in Indian Ocean MORB. *Earth Planet. Sci. Lett.* **147,** 93–106.

Salters V. J. M. (1996) The generation of mid-ocean ridge basalts from the Hf and Nd isotope perspective. *Earth Planet. Sci. Lett.* **141,** 109–123.

Salters V. J. M. and Hart S. R. (1991) The mantle sources of ocean ridges, islands and arcs—The Hf-isotope connection. *Earth Planet. Sci. Lett.* **104,** 364–380.

Salters V. J. M. and Stracke A. (2004) Composition of the depleted mantle. *Geochem. Geophys. Geosyst.* **5,** doi:10.1029/2003 GC000597.

Salters V. J. M. and White W. M. (1998) Hf isotope constraints on mantle evolution. *Chem. Geol.* **145,** 447–460.

Schilling J., Hanan B., McCully B., Kingsley R., and Fontignie D. (1994) Influence of the Sierra-Leone mantle plume on the equatorial Mid-Atlantic Ridge—A Nd-Sr-Pb isotopic study. *J. Geophys. Res.-Solid.* **99,** 12005–12028.

Schilling J., Kingsley R., Fontignie D., Poreda R., and Xue S. (1999) Dispersion of the Jan Mayen and Iceland mantle plumes in the Arctic: A He-Pb-Nd-Sr isotope tracer study of basalts from the Kolbeinsey, Mohns, and Knipovich Ridges. *J. Geophys. Res.-Solid.* **104,** 10543–10569.

Shaw D. M. (1970) Trace element fractionation during anatexis. *Geochim. Cosmochim. Acta* **34,** 237–243.

Sheather S. J. and Jones M. C. (1991) A reliable data-based bandwidth selection method for kernel density estimation. *J. Roy. Statist. Soc.* **B,** 683–690.

Shirey S., Bender J., and Langmuir C. (1987) 3-Component isotopic heterogeneity near the Oceanographer transform, Mid-Atlantic Ridge. *Nature* **325,** 217–223.

Silverman B. W. (1986) *Density Estimation* Chapman and Hall, London.

Sims K. W. W., Goldstein S. J., Blichert-Toft J., Perfit M. R., Kelemen P., Fornari D. J., Michael P., Murrell M. T., Hart S. R., DePaolo D. J., Layne G., Ball L., Jull M., and Bender J. (2002) Chemical and isotopic constraints on the generation and transport of magma beneath the East Pacific Rise. *Geochim. Cosmochim. Acta* **66,** 3481–3504.

Slater L., McKenzie D., Grönvold K., and Shimizu N. (2001) Melt generation and movement beneath Theistareykir, NE Iceland. *J. Petrol.* **42,** 321–354.

Tatsumoto M. (1978) Isotopic composition of lead in oceanic basalt and its implication to mantle evolution. *Earth Planet. Sci. Lett.* **38,** 63–87.

van Keken P. E., Hauri E. H., and Ballentine C. J. (2002) Mantle mixing: The generation, preservation, and destruction of chemical heterogeneity. *Annu. Rev. Earth Planet. Sci.* **30,** 493–525.

Vlastelic I., Aslanian D., Dosso L., Bougault H., Olivet J. L., and Geli L. (1999) Large-scale chemical and thermal division of the Pacific mantle. *Nature* **399,** 345–350.

Wendt J. I., Regelous M., Niu Y. L., Hekinian R., and Collerson K. D. (1999) Geochemistry of lavas from the Garrett Transform Fault: insights into mantle hetero-geneity beneath the Eastern Pacific. *Earth Planet. Sci. Lett.* **173,** 271–284.

White W. M. (1985) Sources of oceanic basalts: Radiogenic isotopic evidence. *Geology* **13,** 115–118.

White W. M. (1993) $^{238}U/^{204}Pb$ in MORB and open system evolution of the depleted mantle. *Earth Planet. Sci. Lett.* **115,** 211–226.

White W. M., Hofmann A. W., and Puchelt H. (1987) Isotope geochemistry of Pacific midocean ridge basalt. *J. Geophys. Res.-Solid.* **92,** 4881–4893.

Xie S. and Tackley P. J. (2004) Evolution of U-Pb and Sm-Nd systems in numerical models of mantle convection and plate tectonics. *J. Geophys. Res.* **109,** B11204, doi:10.1029/2004JB003176.

Yu D., Fontignie D., and Schilling J. G. (1997) Mantle plume-ridge interactions in the Central North Atlantic: A Nd isotope study of Mid-Atlantic Ridge basalts from 30°N to 50°N. *Earth Planet Sci. Lett.* **146,** 259–272.

Zindler A. and Hart S. R. (1986) Chemical geodynamics. *Ann. Rev. Earth Planet. Sci.* **14,** 493–571.

Zou H. (1998) Trace element fractionation during modal and nonmodal dynamic melting and open-system melting: A mathematical treatment. *Geochim. Cosmochim. Acta* **62,** 1937–1945.

A. THE BASIC MODEL

A.1. Radioactive Decay

We track the molar concentrations of the three isotopes p, d, and d'. Consider a fluid parcel which remains outside the melting region. Suppose we have $p = p_{start}$, $d = d_{start}$, and $d' = d'_{start}$ for such a fluid parcel. Following this fluid parcel we have

$$\frac{\mathrm{D}p}{\mathrm{D}t} = -\lambda p \qquad \frac{\mathrm{D}d}{\mathrm{D}t} = -\lambda p \qquad \frac{\mathrm{D}d'}{\mathrm{D}t} = 0 \qquad \text{(A.1)}$$

Thus, after a time t following this fluid parcel we have

$$p = p_{start}e^{-\lambda t}$$
$$d = d_{start} + p_{start}(1 - e^{-\lambda t})$$
$$d' = d'_{start} \qquad \text{(A.2)}$$

and in particular

$$\left(\frac{d}{d'}\right) = \left(\frac{d}{d'}\right)_{\text{start}} + (1 - e^{-\lambda t})\left(\frac{p}{d'}\right)_{\text{start}} \qquad (A.3)$$

Suppose that $\lambda t \ll 1$. Then approximating this to first order we have

$$\left(\frac{d}{d'}\right) = \left(\frac{d}{d'}\right)_{\text{start}} + \lambda t\left(\frac{p}{d'}\right)_{\text{start}} \qquad (A.4)$$

Let $\bar{p}_0$, $\bar{d}_0$, and $\bar{d}'_0$ be the mean concentrations of these isotopes over the whole box at the present day. Let $\bar{p}_\tau$, $\bar{d}_\tau$, and $\bar{d}'_\tau$ be the same mean concentrations an age τ ago. Then working in similar way but integrating backwards in time, if $\lambda\tau \ll 1$ we have

$$\left(\frac{\bar{d}}{\bar{d}'}\right)_\tau = \left(\frac{\bar{d}}{\bar{d}'}\right)_0 - \lambda\tau\left(\frac{\bar{p}}{\bar{d}'}\right)_0 \qquad (A.5)$$

The assumption that the age is short compared to the radioactive decay time scale means we can treat (p/d') as a constant and look at linear growth of (d/d').

A.2. Melting

At intervals Δt a melting event occurs in the melting region. In a melting event we find the mean values of p, d, and d' in the melting region and call these our p_{source}, d_{source}, and d'_{source} values. Note that in the steady state approximation the mean of the melting region is the same as the mean over the whole box. That is to say $p_{\text{source}} = \bar{p}_\tau$, $d_{\text{source}} = \bar{d}_\tau$, and $d'_{\text{source}} = \bar{d}_\tau'$ at an age τ before the present day.

The melting region produces a melt fraction F of melt. As such, a fraction F of material in the melting region is set with $p = p_{\text{melt}}$, $d = d_{\text{melt}}$, and $d' = d'_{\text{melt}}$, where these values are calculated from the expressions below. Similarly, a fraction $(1 - F)$ is set to the appropriate residue values. The melting equations are

$$p_{\text{melt}} = \frac{G_p}{F} p_{\text{source}} \qquad p_{\text{res}} = \frac{1 - G_p}{1 - F} p_{\text{source}}$$

$$d_{\text{melt}} = \frac{G_d}{F} d_{\text{source}} \qquad d_{\text{res}} = \frac{1 - G_d}{1 - F} d_{\text{source}} \qquad (A.6)$$

$$d'_{\text{melt}} = \frac{G_{d'}}{F} d'_{\text{source}} \qquad d'_{\text{res}} = \frac{1 - G_{d'}}{1 - F} d'_{\text{source}}$$

where G_p, G_d, and $G_{d'}$ come from the melting model used and are related to the partition coefficients for the relevant isotopes and the melt fraction F. A good overview of different melt models is given in Zou (1998). Here we have used the Shaw (1970) model, where

$$G_p = 1 - \left(1 - \frac{P_p}{D_p}F\right)^{1/P_p} \qquad (A.7)$$

with similar definitions for G_d and $G_{d'}$. This is slightly confusing notation—upper case P and D are different weighted averages of partition coefficients for a given isotope, whereas lower case p and d refer to the parent and daughter isotopes, respectively.

$$D_p = \sum_i x^i K_p^i$$

$$P_p = \sum_i q^i K_p^i \qquad (A.8)$$

K_p^i is the mineral/melt partition coefficient for the parent in mineral i; x^i is the mass fraction of mineral i in the source rock; and q^i is the fractional contribution of mineral i to the melt. Note that

$$G_p \to \frac{F}{D_p} \quad \text{as} \quad F \to 0 \qquad (A.9)$$

We will assume that isotopes of the same element have the same behavior under melting (and thus for a given melt fraction the same G), and in particular that $G_d = G_{d'}$. With $\lambda\tau \ll 1$ we can treat the $(p/d')_{\text{melt}}$ and $(p/d')_{\text{res}}$ values as constants. Therefore, at an age τ before the present day we have

$$\left(\frac{p}{d'}\right)_{\text{melt}} = \frac{G_p}{G_d}\left(\frac{\bar{p}}{\bar{d}'}\right)_0$$

$$\left(\frac{p}{d'}\right)_{\text{res}} = \frac{1 - G_p}{1 - G_d}\left(\frac{\bar{p}}{\bar{d}'}\right)_0 \qquad (A.10)$$

$$\left(\frac{d}{d'}\right)_{\text{melt}} = \left(\frac{d}{d'}\right)_{\text{res}} = \left(\frac{\bar{d}}{\bar{d}'}\right)_0 - \lambda\tau\left(\frac{\bar{p}}{\bar{d}'}\right)_0$$

A.3. Rates of Growth

Define the age τ of a parcel as the time elapsed since the parcel last entered the melting region. Any given parcel was last created either as melt or residue in the melting region. Because the melt fraction produced by the melting region is F, this means a fraction F of the overall material will have come from melt and $(1 - F)$ from residue. Suppose a parcel has an age τ and was made as melt a time τ ago. Then its present (d/d') value is

$$\left(\frac{d}{d'}\right)_{\tau,\text{was melt}} = \left(\frac{d}{d'}\right)_{\text{melt}} + \lambda\tau\left(\frac{p}{d'}\right)_{\text{melt}}$$

$$= \left(\frac{\bar{d}}{\bar{d}'}\right)_0 + \lambda\tau\left(\left(\frac{p}{d'}\right)_{\text{melt}} - \left(\frac{\bar{p}}{\bar{d}'}\right)_0\right) \qquad (A.11)$$

This can be simplified as

$$\left(\frac{d}{d'}\right)_{\tau,\text{was melt}} = \left(\frac{d}{d'}\right)_0 - \frac{\nu\tau}{G_d} \qquad (A.12)$$

where

$$\nu = \lambda(G_d - G_p)\left(\frac{\bar{p}}{\bar{d}'}\right)_0 \qquad (A.13)$$

Similarly for the residue we have

$$\left(\frac{d}{d'}\right)_{\tau,\text{was res}} = \left(\frac{\bar{d}}{\bar{d}'}\right)_0 + \frac{\nu\tau}{1 - G_d} \qquad (A.14)$$

A.4. Distribution of Ages

Let the melting region have nondimensional area A relative to the size of the box. Define the iterate age s to be the number of iterates since a given parcel last entered the melting region. Let $\hat{S}$ be a discrete random variable giving the distribution of iterate ages. If the advection is strongly stirring, then the probability of any given parcel entering the melting region at that timestep is A. Considering a long time statistical steady state, $\hat{S}$ is given by a geometric distribution, where the probability of an iterate age of s is

$$A(1 - A)^s \quad s = 0, 1, 2\ldots \qquad (A.15)$$

However, it is easier to work with a continuous distribution. The continuous analog of the geometric distribution is the exponential distribution. The age τ is the time since a given parcel last entered the melting region, so $\tau = s\Delta t$. Note that

$$A(1 - A)^s = A\exp\left(-\tau\frac{-\log(1 - A)}{\Delta t}\right) \qquad (A.16)$$

So the discrete distribution has an associated melting time scale given by

$$\tau_{\text{melt}} = \frac{\Delta t}{-\log(1 - A)} \qquad (A.17)$$

Taking the limit as $\Delta t \to 0$, $A \to 0$ with τ_{melt} fixed allows us to relate the discrete and continuous distributions. Let $\hat{T}$ be the continuous random variable giving the distribution of ages. Then $\hat{T}$ is distributed exponentially with mean τ_{melt}. Let $\hat{E}$ be an exponential random variable with mean 1. Then we can write $\hat{T} = \tau_{\text{melt}} \hat{E}$. $\hat{E}$ has probability density function given by

$$f_{\hat{E}}(x) = e^{-x} \quad x > 0 \tag{A.18}$$

In this limit the time interval Δt and the melting region area A become infinitesimal. As such the assumption that strong stirring occurs between time intervals cannot be made. However, the continuous limit should be a reasonable approximation provided the time scale for stirring is short compared to the melting time scale τ_{melt}, and for calculational convenience it is used from now on.

A.5. Distribution of d/d'

In terms of the random variable $\hat{T}$ giving the distribution of ages we have (using Eqns. A.12 and A.14) the following for the distribution of d/d' in the interior of the box

$$\left(\frac{\hat{d}}{\hat{d}'}\right) - \left(\frac{\overline{d}}{\overline{d}'}\right)_0 \sim \begin{cases} -\nu\hat{T}/G_d & \text{(melt)} \\ \nu\hat{T}/(1-G_d) & \text{(res)} \end{cases} \tag{A.19}$$

where we have a probability F of getting a melt value, and $(1 - F)$ of getting a residue value. Here hats on $\hat{d}$ and $\hat{d}'$ are used to denote that they are random variables. Eqn. A.19 can also be expressed in terms of the exponential random variable $\hat{E}$ as

$$\left(\frac{\hat{d}}{\hat{d}'}\right) - \left(\frac{\overline{d}}{\overline{d}'}\right)_0 \sim \begin{cases} -l\hat{E}/G_d & \text{(melt)} \\ l\hat{E}/(1-G_d) & \text{(res)} \end{cases} \tag{A.20}$$

where

$$l = \nu\tau_{\text{melt}} = \lambda\tau_{\text{melt}}(G_d - G_p)\left(\frac{\overline{p}}{\overline{d}'}\right)_0 \tag{A.21}$$

B. SAMPLING

When we sample the mantle we do not sample directly from the distribution that has just been derived. In fact we sample after numerous components from this distribution have melted and mixed together. This is the "sampling under melting and averaging" (SUMA) concept (Meibom and Anderson, 2003). We will assume there is no bias in melting and mixing: The likelihood of a component entering the melt is proportional to its abundance in the source.

Suppose we mix together N independent random samples from the distribution of Eqn. A.20. Note in particular that the (d/d') ratio of the mixture is *not* the mean of the ratios of the independent samples. Instead, the individual concentrations d and d' are averaged and the ratio is then calculated, i.e., the quantity of interest is

$$\sum_{i=1}^{N} d_i \bigg/ \sum_{i=1}^{N} d_i' \tag{B.1}$$

Note in particular the following identity

$$\frac{\sum_{i=1}^{N} d_i}{\sum_{i=1}^{N} d_i'} - \left(\frac{\overline{d}}{\overline{d}'}\right)_0 = \sum_{i=1}^{N} w_i \left[\left(\frac{d_i}{d_i'}\right) - \left(\frac{\overline{d_i}}{\overline{d_i}'}\right)_0\right] \tag{B.2}$$

where the weights w_i are given by

$$w_i = d_i' \bigg/ \sum_{i=1}^{N} d_i' \tag{B.3}$$

Let $\hat{Z}$ give the distribution of $(\sum_{i=1}^{N} \hat{d}_i / \sum_{i=1}^{N} \hat{d}_i')$ and $\hat{R}_i$ give the distribution of $(\hat{d}_i/\hat{d}_i') - (\overline{d}/\overline{d}')_0$. Then the $\hat{R}_i$'s are independent identically distributed (i.i.d.) random variables with distribution (using Eqn. A.20)

$$\hat{R}_i = \begin{cases} -l\hat{E}/G_d & \text{(melt)} \\ l\hat{E}/(1-G_d) & \text{(res)} \end{cases} \tag{B.4}$$

where the $\hat{E}_i$'s are i.i.d. exponential random variables with mean 1.

Now, note that $\hat{d}_i'$ can only take two values in our model: It is $\overline{d}_0' G_d/F$ if we have a melt value, and $\overline{d}_0' (1 - G_d)/(1 - F)$ if we have a residue value. Therefore,

$$\hat{d}_i'\hat{R}_i = \begin{cases} -\overline{d}_0'l\hat{E}_i/F & \text{(melt)} \\ \overline{d}_0'l\hat{E}_i/(1-F) & \text{(res)} \end{cases} \tag{B.5}$$

Now $\sum_{j=1}^{N} d_j'$ depends on how many melt and how many residue components are mixed together. Suppose we have r melt components and $N - r$ residue components in the mix. Then $\sum_{j=1}^{N} d_j' = M(r) \overline{d}_0'$ where

$$M(r) = r\frac{G_d}{F} + (N - r)\frac{1 - G_d}{1 - F} \tag{B.6}$$

Assuming the sampling is unbiased, the probability q_r of getting r melt components and $N - r$ residue components in the mix is given by the binomial distribution

$$q_r = \binom{N}{r}F^r(1 - F)^{N-r} \tag{B.7}$$

Therefore, $\hat{Z}$ has distribution given by

$$\hat{Z} = \hat{Y}_r \quad \text{with probability } q_r \tag{B.8}$$

where $\hat{Y}_r$ is the result of combining r melt and $N - r$ residue components, with distribution given in terms of the $\hat{E}_i$'s as

$$\hat{Y}_r = \frac{1}{M(r)}\left(\sum_{i=1}^{r} -\frac{\hat{E}_i}{F} + \sum_{i=r+1}^{N} \frac{\hat{E}_i}{1-F}\right) \tag{B.9}$$

The above expression forms the basis of one method of estimating the density function for d/d' after sampling. Exponential random variables can be simulated easily, so an artificial sample from this distribution can be constructed. From this it is possible to numerically estimate the density (e.g. by kernel smoothing, Appendix D).

B.1. Characteristic Functions

In order to get an analytic expression for the probability distribution of $\hat{Z}$ it is useful to use characteristic functions. Suppose a random variable has probability density function $f(x)$. Then its characteristic function $\phi(k)$ is defined by its Fourier transform

$$\phi(k) = \int_{-\infty}^{\infty} e^{-ikx}f(x)dx \tag{B.10}$$

There are two important properties that we wish to exploit. If $\hat{X}$ is a random variable with characteristic function $\phi(k)$ then $a\hat{X}$ has characteristic function $\phi(ak)$. Also, if $\hat{X}_1$, $\hat{X}_2$, ... $\hat{X}_n$ are independently distributed with characteristic functions $\phi_1(k)$, $\phi_2(k)$, ... $\phi_n(k)$, then $\sum_{i=1}^{n} \hat{X}_i$ has characteristic function $\prod_{i=1}^{n} \phi_i(k)$.

The exponential random variable $\hat{E}$ has characteristic function

$$\phi_{\hat{E}}(k) = (1 + ik)^{-1} \tag{B.11}$$

Therefore, using the two properties stated above, $\hat{Y}_r$ has characteristic function

$$\phi_{\hat{Y}_r}(k) = \left(1 - \frac{ikl}{M(r)F}\right)^{-r}\left(1 + \frac{ikl}{M(r)(1-F)}\right)^{-(N-r)} \tag{B.12}$$

Therefore $\hat{Z}$ has characteristic function

$$\phi_{\hat{Z}}(k) = \sum_{r=0}^{N} \binom{N}{r}F^r(1-F)^{N-r} \phi_{\hat{Y}_r}(k) \tag{B.13}$$

By using the Fourier inversion theorem we may recover the distribution of $\hat{Z}$.

$$f_{\hat{Z}}(x) = \frac{1}{2\pi} \int_{-\infty}^{\infty} e^{ikx} \phi_{\hat{Z}}(k) dk \qquad \text{(B.14)}$$

This is another way of constructing the density of d/d' after sampling, and it gives the precise density function. Doing this Fourier inversion analytically leads to complicated sums of a large number of terms. These are very time consuming to calculate, and difficult to interpret. However, this integral can be done efficiently numerically using a Fast Fourier Transform (FFT), and this method was used to produce Fig. 2. Moreover, simpler asymptotic results for large N can be obtained that are easier to interpret and much quicker to evaluate.

C. ASYMPTOTIC RESULTS

C.1 Asymptotic Moments

The moments of the distribution can be read off from the Taylor expansion about $k = 0$ of the characteristic function. If the nth moment is α_n we have

$$\phi_{\hat{Z}}(k) = \sum_{n=0}^{\infty} \alpha_n \frac{(-ik)^n}{n!} \qquad \text{(C.1)}$$

We are interested in understanding the behavior of these moments for large N. Note that the characteristic function can be written as

$$\phi_{\hat{Z}}(k) = \sum_{r=0}^{N} \binom{N}{r} F^r (1-F)^{N-r} v\left(\frac{r}{N}\right) \qquad \text{(C.2)}$$

where

$$v(x) = \left(1 - \frac{ikl}{NFm(x)}\right)^{-Nx} \left(1 + \frac{ikl}{N(1-F)m(x)}\right)^{-N(1-x)} \qquad \text{(C.3)}$$

and

$$m(x) = x\frac{G_d}{F} + (1-x)\frac{1-G_d}{1-F} \qquad \text{(C.4)}$$

Taylor expanding $v(r/N)$ in Eqn. C.2 about $r/N = F$ (the mean of the binomial distribution) gives

$$\phi_{\hat{Z}}(k) = v(F) + \frac{F(1-F)}{2N} v''(F) + \frac{F(1-F)(1-2F)}{6N^2} v'''(F)$$
$$+ \frac{3F^2(1-F)^2}{24N^2} v^{(4)}(F) + O\left(\frac{1}{N^3}\right) \qquad \text{(C.5)}$$

where the coefficient of $v^{(m)}(F)$ is simply the mth central moment of the binomial distribution over $m!N^m$.

Taylor expanding $v(x)$ given in Eqn. C.3 about $k = 0$ yields

$$v(x) = 1 + (-ikl)\frac{F-x}{(1-G_d)F + (G_d-F)x}$$
$$+ \frac{(-ikl)^2}{2} \frac{N(F-x)^2 + F^2 + x - 2Fx}{N((1-G_d)F + (G_d-F)x)^2} + \cdots \qquad \text{(C.6)}$$

Taylor expanding this expression for $v(x)$ about $x = F$ and substituting into equation Eqn. C.5 allows us to read off the asymptotic moments. To leading order we have

$$\bar{Z} = E[\hat{Z}] = l\left(\frac{G_d-F}{NF(1-F)} + O\left(\frac{1}{N^2}\right)\right)$$

$$E[(\hat{Z}-\bar{Z})^2] = l^2\left(\frac{2}{NF(1-F)} + O\left(\frac{1}{N^2}\right)\right) \qquad \text{(C.7)}$$

$$E[(\hat{Z}-\bar{Z})^3] = l^3\left(\frac{6(2G_d-1)}{(NF(1-F))^2} + O\left(\frac{1}{N^3}\right)\right)$$

In particular, note that the skew parameter γ_1 is

$$\gamma_1 = E[(\hat{Z}-\bar{Z})^3]/(E[(\hat{Z}-\bar{Z})^2])^{3/2}$$
$$= \text{sgn}(l)\left(\frac{3(2G_d-1)}{(2NF(1-F))^{1/2}} + O\left(\frac{1}{N^{3/2}}\right)\right) \qquad \text{(C.8)}$$

Most importantly from all this we see that the asymptotic standard deviation $\sigma = \sqrt{\text{van}(\hat{Z})}$ of this distribution is

$$\sigma \approx \lambda \tau_{\text{melt}} |G_d - G_p| \left(\frac{\bar{p}}{\bar{d'}}\right)_0 \sqrt{\frac{2}{NF(1-F)}} \qquad \text{(C.9)}$$

Less important is the small $O(1/N)$ correction to the mean which is not significant compared with the $O(1/N^{1/2})$ standard deviation. Higher order moments and corrections can be easily found by just expanding the Taylor series to higher orders.

C.2 Asymptotic Density: Edgeworth Expansion

An approximate form of the density for large N can obtained by using an Edgeworth expansion (see Blinnikov and Moessner (1998) for a fuller discussion of these expansions). Let $\hat{Q} = (\hat{Z} - \bar{Z})/\sigma$. Then the first two terms in the Edgeworth expansion for the density of $\hat{Q}$ is

$$f_{\hat{Q}}(x) = \frac{e^{-x^2/2}}{\sqrt{2\pi}} \left\{ 1 + \sigma\frac{S_3}{6}\text{He}_3(x) \right.$$
$$\left. + \sigma^2\left(\frac{S_4}{24}\text{He}_4(x) + \frac{S_3^2}{72}\text{He}_6(x)\right) + O(\sigma^3) \right\} \qquad \text{(C.10)}$$

where $S_n = \kappa_n/\sigma^{2n-2}$ and κ_n is the nth cumulant defined by

$$\log\phi_{\hat{Z}}(k) = \sum_{n=0}^{\infty} \kappa_n \frac{(-ik)^n}{n!} \qquad \text{(C.11)}$$

and $\text{He}_n(x)$ is the nth Chebyshev-Hermite polynomial, the relevant ones being

$$\text{He}_3(x) = x^3 - 3x$$
$$\text{He}_4(x) = x^4 - 6x^2 + 3$$
$$\text{He}_6(x) = x^6 - 15x^4 + 45x^2 - 15 \qquad \text{(C.12)}$$

and

$$\sigma = |l| \sqrt{\frac{2}{NF(1-F)}} + O\left(\frac{1}{N^{3/2}}\right) \qquad \text{(C.13)}$$

Using the results of the previous section we can calculate the cumulants of the distribution in powers of σ. Thus

$$S_3 = \frac{\kappa_3}{\sigma^4} = \frac{3}{2l}(2G_d - 1) + O(\sigma^2)$$

$$S_4 = \frac{\kappa_4}{\sigma^6} = \frac{3}{2l^2}(14G_d^2 + F^2 - 8FG_d - 10G_d + 3F + 2) + O(\sigma^2)$$

$$\text{(C.14)}$$

Substituting these expressions back in to Eqn. C.10 gives an expansion with errors of $O(\sigma^3)$. Substituting back the leading order expression for σ (Eqn. C.13) gives an expansion in powers of N with errors of

$O(1/N^{3/2})$. As an example, working to first order in σ (as the next term is more cumbersome) we get

$$f_{\hat{Q}}(x) = \frac{e^{-x^2/2}}{\sqrt{2\pi}}\left\{1 + \frac{(2G_d - 1)\text{sgn}(l)}{2\sqrt{2NF(1-F)}}\,\text{He}_3(x) + O\left(\frac{1}{N}\right)\right\} \quad \text{(C.15)}$$

The above Edgeworth expansion is a third way of estimating the distribution of d/d' after sampling. Its main strength is that it is the quickest to evaluate. It is an approximation to the true density and can contain features that the true density would not. For example, it is possible for an Edgeworth expansion of a density to become negative, although it still always integrates to 1.

C.3 Mixing Lines

Consider two isotopic systems (1) and (2) with potentially different parent and daughter elements. Suppose we plot $(d/d')^{(2)}$ against $(d/d')^{(1)}$. We are interested in knowing where our samples plot.

Consider a sample which was made by averaging r melt components and $N - r$ residue components. Recall

$$\widehat{Y}_r^{(1)} = \frac{l^{(1)}}{M^{(1)}(r)}\left(\sum_{i=1}^{r} -\frac{\widehat{E}_i}{F} + \sum_{i=r+1}^{N} \frac{\widehat{E}_i}{1-F}\right) \quad \text{(C.16)}$$

and note in particular that the part in brackets is independent of isotopic system and melt model.

Therefore

$$\frac{\widehat{Y}_r^{(2)}}{\widehat{Y}_r^{(1)}} = \frac{l^{(2)}M^{(1)}(r)}{l^{(1)}M^{(2)}(r)} = \beta_r \quad \text{(C.17)}$$

That is, in a plot of $(d/d')^{(2)}$ against $(d/d')^{(1)}$ samples will lie on straight lines through $((\overline{d/d'})_0^{(1)}, (\overline{d/d'})_0^{(2)})$ with gradients β_r. For example, when $r = 0$ we have

$$\beta_0 = \frac{l^{(2)}\left(1 - G_d^{(1)}\right)}{l^{(1)}\left(1 - G_d^{(2)}\right)} \quad \text{(C.18)}$$

and when $r = N$ we have

$$\beta_N = \frac{l^{(2)}G_d^{(1)}}{l^{(1)}G_d^{(2)}} \quad \text{(C.19)}$$

For large N, we can use the methods of expansion used in the previous section to show that for

$$\widehat{\beta} = \beta_r \qquad \text{with probability } q_r \quad \text{(C.20)}$$

we have

$$\overline{\beta} = E(\widehat{\beta}) = \frac{l^{(2)}}{l^{(1)}} + O\left(\frac{1}{N}\right) \quad \text{(C.21)}$$

and

$$\text{var}(\widehat{\beta}) = \left(\frac{l^{(2)}}{l^{(1)}}\right)^2 \frac{\left(G_d^{(1)} - G_d^{(2)}\right)^2}{NF(1-F)} + O\left(\frac{1}{N^2}\right) \quad \text{(C.22)}$$

So for N large the mean gradient of the lines can be approximated to leading order by $l^{(2)}/l^{(1)}$. Therefore

$$\overline{\beta} \approx \frac{\lambda^{(2)}\left(G_d^{(2)} - G_p^{(2)}\right)\left(\overline{p}/\overline{d'}\right)_0^{(2)}}{\lambda^{(1)}\left(G_d^{(1)} - G_p^{(1)}\right)\left(\overline{p}/\overline{d'}\right)_0^{(1)}} \quad \text{(C.23)}$$

Note a particular special case: If for both systems the daughters are isotopes of the same element (for example, both isotopes of lead), then $M^{(1)}(r) = M^{(2)}(r)$ and all samples lie on a single straight line of gradient exactly $\beta = l^{(2)}/l^{(1)}$. In this case it is usual for the reference isotopes to be the same $d'^{(1)} = d'^{(2)}$. Furthermore, if it is also the case that the parent elements are the same (or at least behave similarly under
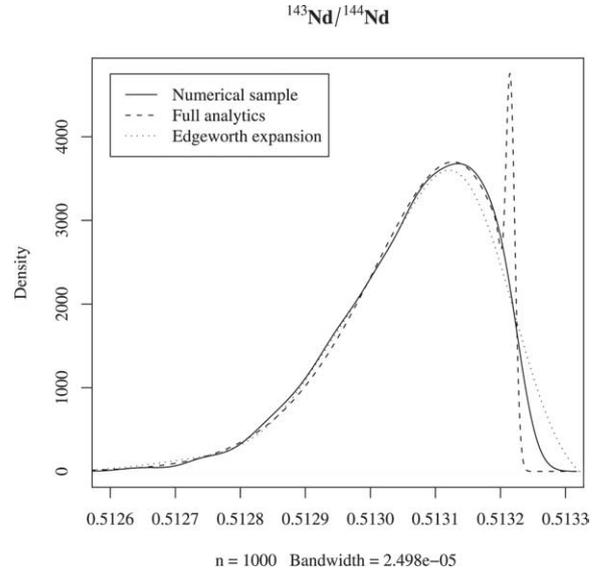

Fig. D.1. Plot comparing the three methods of density estimation in the model for ^{143}Nd/^{144}Nd, with $F = 0.5\%$, $\tau_{\text{melt}} = 1.7$ Ga, and $N = 500$. For the numerical sample, the sample size n is shown along with the bandwidth of the kernel smoother. The Edgeworth expansion is to second order (up to and including terms of order σ^2).

melting, $G_p^{(1)} \approx G_p^{(2)}$) then this gradient is independent of the melt model and is simply

$$\beta = \frac{\lambda^{(2)}}{\lambda^{(1)}}\left(\frac{\overline{p}^{(2)}}{\overline{p}^{(1)}}\right)_0 \quad \text{(C.24)}$$

D. COMPARISON OF METHODS FOR DENSITY ESTIMATION

We have outlined in the previous sections (B, B.1, and C.2) three methods of estimating the density of d/d' in the model. The first method, numerical simulation, generates a sample from the model distribution by using computer-generated samples from an exponential distribution. The probability density is then estimated using a kernel smoothed estimate for this sample. Given n independent observations $x_1, x_2, \ldots, x_n$ from the random variable $\widehat{X}$, the kernel density estimator $\widetilde{f}_h(x)$ of the density value $f(x)$ is defined as

$$\widetilde{f}_h(x) = \frac{1}{nh}\sum_{i=1}^{n} K\left(\frac{x_i - x}{h}\right) \quad \text{(D.1)}$$

where h is the bandwidth and $K(u)$ the kernel function. For a gaussian kernel

$$K(u) = \frac{1}{\sqrt{2\pi}}\exp\left(-\frac{1}{2}u^2\right) \quad \text{(D.2)}$$

The function DENSITY in R (R Development Core Team (2004)) was used to calculate this efficiently. One advantage of using kernel-smoothed estimates, for example, over plotting a histogram, is that it is easy to plot more than one density on the same plot. In this work, the default gaussian kernel was used, with optimal bandwidth as chosen by R. Kernel-smoothed estimates are sensitive to choices of kernel and bandwidth; see Sheather and Jones (1991), Silverman (1986), and the R documentation for a fuller discussion.

The second method involves calculating the full analytic distribution by numerically doing the Fourier inversion of Eqn. B.14. The advantage of this method is that you get the density precisely.

The third method is to use the asymptotic approximation provided by the Edgeworth expansion of Eqn. C.15. This is an approximation to the

Table F.1. Elemental concentrations, garnet/spinel partition coefficients and isotopic abundances.

	^{147}Sm	^{87}Rb	^{176}Lu	^{232}Th	^{238}U	^{235}U
parent isotope p	^{147}Sm	^{87}Rb	^{176}Lu	^{232}Th	^{238}U	^{235}U
daughter isotope d	^{143}Nd	^{87}Sr	^{176}Hf	^{208}Pb	^{206}Pb	^{207}Pb
reference isotope d'	^{144}Nd	^{86}Sr	^{177}Hf	^{204}Pb	^{204}Pb	^{204}Pb
parent element conc./ppm[a]	0.272	0.0930	0.0550	0.00420	0.00170	0.00170
daughter element conc./ppm[a]	0.677	14.0	0.237	0.0150	0.0150	0.0150
par./dau. elemental ratio[a]	0.402	0.00664	0.232	0.280	0.113	0.113
p isotope abundance /%[b]	15.0	27.84	2.60	100.0	99.27	0.72
d' isotope abundance /%[b]	23.8	9.86	18.6	1.40	1.40	1.40
parent D_{spinel}[a]	0.03477	0.00039	0.05077	0.00016	0.00012	0.00012
parent P_{spinel}[a]	0.10634	0.00056	0.12193	0.00052	0.00036	0.00036
parent D_{garnet}[a]	0.04760	0.00039	0.66733	0.00028	0.00118	0.00118
parent P_{garnet}[a]	0.15028	0.00062	2.18507	0.00091	0.00391	0.00391
daughter D_{spinel}[a]	0.02778	0.03454	0.02888	0.03198	0.03198	0.03198
daughter P_{spinel}[a]	0.08592	0.10403	0.08878	0.08393	0.08393	0.08393
daughter D_{garnet}[a]	0.02801	0.02277	0.06939	0.02186	0.02186	0.02186
daughter P_{garnet}[a]	0.08745	0.06666	0.22516	0.05348	0.05348	0.05348

[a] McKenzie and O'Nions (1991).
[b] Lide (2003).

true density, but is the quickest of the three methods to calculate, and becomes more accurate as N is increased.

Figure D.1 uses these three methods to produce model densities for ^{143}Nd/^{144}Nd. All three methods produce very similar shapes, clearly showing similar standard deviations and skews. The analytic density contains a small scale spike at 0.51322. The area under this spike is small compared with 1. The spike is not seen in the kernel-smoothed estimate because it is a feature of a scale smaller than the bandwidth. Similarly it is not seen in the Edgeworth expansion because there are not enough terms in the expansion to express such a feature. Our interest in this work is in broad features of the distributions, and such small features are liable to be disturbed by other factors (for example, measurement error), so this spike is not an important feature. Note also that the Edgeworth expansion becomes negative on the far right of the plot, which is a disadvantage in using such an expansion far from the mean.

When demonstrating the behaviour of the model distribution with varying N in Figure 2, numerical Fourier inversion was used for greatest accuracy. However, when comparing the model with measured data in Figure 3 we have opted to use kernel-smoothed densities to provide a more like-for-like comparison between the model and measured data. When generating a model sample, a sample size of 1000 was used to provide a close comparison with the measured data used, which is of a similar size.

E. REMARKS ON THE CENTRAL LIMIT THEOREM

As has been discussed in section B, when we sample from our model mantle we do so after averaging a number of components. For a set of independent identically distributed random variables $X_1, X_2, \ldots, X_N$ with mean μ_0 and standard deviation σ_0, the central limit theorem states that the distribution of $\bar{X} = \Sigma X_i / N$ will approach a normal distribution with mean μ_0 and standard deviation $\sigma_0/\sqrt{N}$. However, this cannot be applied in mixing isotopic ratios, because it is the individual concentrations of d and d' that are averaged and then the ratio taken. Hence $\bar{d}/\bar{d'} = \Sigma d_i/\Sigma d_i' \neq \Sigma(d_i/d_i')/N$. As always in geochemistry, great care must be taken in dealing with ratios of quantities. However, it does turn out that in our model we do approach a normal distribution, but the standard deviation is quite different from a naive use of the central limit theorem. As an example, using Meibom and Anderson's (2003) notation, the standard deviation σ_{um} of the d/d' distribution before averaging is

$$\sigma_{um} = |l| \frac{\sqrt{(F - G_d)^2 + 2F(1 - F)}}{G_d(1 - G_d)} \tag{E.1}$$

whereas the standard deviation σ_{meas} we would measure after the averaging is

$$\sigma_{meas} = |l| \left(\sqrt{\frac{2}{NF(1 - F)}} + O\left(\frac{1}{N^{3/2}}\right) \right) \tag{E.2}$$

and in particular it is clear that

$$\sigma_{meas} \neq \frac{\sigma_{um}}{\sqrt{N}} \tag{E.3}$$

In fact, for the model values for Nd, there is a factor of 15 difference between the left and right hand sides of the above expression when N is large. It is also important to note that the approach to a normal distribution is governed by $N F (1 - F)$ and not N, as indicated by the expression for the skew of the distribution (Eqn. 4) and the first correction to the normal distribution in the Edgeworth expansion (Eqn. C.10). Because F is small, the distributions we observe are significantly skewed despite N being large.

F. DATA SOURCES

Table F.1 gives the raw data from which some of the data in Table 1 was calculated. The weighted partition coefficients P and D given in Table 1 are a linear combination of 60% of the garnet and 40% of the spinel coefficients given in Table F.1.

The MORB data set was a compilation by A. Stracke from the work of Bach et al. (1994), Chauvel and Blichert-Toft (2001), Dosso et al. (1988, 1993, 1999, 1991), Douglass et al. (1999), Fontignie and Schilling (1996), Frey et al. (1993), Hamelin and Allègre (1985), Hamelin et al. (1986), Hanan et al. (1986), Hegner and Tatsumoto (1987), Ito et al. (1987), Kempton et al. (2000), Klein et al. (1991, 1988), MacDougall and Lugmair (1986), Mahoney et al. (2002, 1989, 1994), Mertz et al. (1991), Mertz and Haase (1997), Michard et al. (1986), Newsom et al. (1986), Price et al. (1986), Pyle et al. (1992), Rehkämper and Hofmann (1997), Salters (1996), Salters and Hart (1991), Salters and White (1998), Schilling et al. (1994, 1999), Shirey et al. (1987), Sims et al. (2002), Vlastelic et al. (1999), Wendt et al. (1999), White et al. (1987), and Yu et al. (1997).